Discordance Dating: A New Approach for Dating Alteration Events

Jesse R Reimink[1*]; Renan Beckman[1]; Erik Schoonover[1]; Max Lloyd[1]; Joshua Garber[1]; Joshua HFL Davies[2]; Alexander Cerminaro[1,3]; Morgann G Perrot[2,4]; Andrew Smye[1]

[1]Department of Geosciences, The Pennsylvania State University, University Park, PA, USA
[2]Département des sciences de la Terre et de l'atmosphère / GEOTOP, Université du Québec à Montréal, Montréal, CA
[3]Department of Geosciences, Texas Tech University, 1200 Memorial Circle, Lubbock, TX, USA
[4]Department of Earth and Planetary Sciences, McGill University, Montréal, CA
*corresponding author: jreimink@psu.edu

Abstract:
Zircon is the premier geochronometer used to date igneous and metamorphic processes, constrain sediment provenance, and monitor key events in Earth history such as the growth of continents and the evolution of the biosphere. Zircon U-Pb systematics can be perturbed by the loss or gain of uranium and/or lead, which can result in disagreement between the apparent radiometric ages of the two U-Pb decay systems – a phenomenon that is commonly termed 'discordance'. Discordance in zircon can be difficult to reliably interpret and therefore discordant data are traditionally culled from U-Pb isotopic datasets, particularly detrital zircon datasets. Here we provide a data reduction scheme that extracts reliable age information from discordant zircon U-Pb data found in detrital zircon suites, tracing such processes as fluid flow or contact metamorphism. We provide the template for data reduction and interpretation, a suite of sensitivity tests using synthetic data, and ground-truth this method by analyzing zircons from the well-studied Alta Stock metamorphic aureole. Our results show accurate quantification of a ~24 Ma in situ zircon alteration event that affected 1.0-2.0 Ga detrital zircons in the Tintic quartzite. The 'discordance dating' method outlined here may be widely applicable to a variety of detrital zircon suites where pervasive fluid alteration or metamorphic recrystallization has occurred, even in the absence of concordant U-Pb data.

1. Introduction:
Discordant zircon U-Pb data may be created in multiple ways, including pure Pb-loss (Nasdala et al., 1998), uranium addition (Garber et al., 2020; Grauert et al., 1974; Seydoux-Guillaume et al., 2015), a combination of both U gain and Pb loss (Andersen and Elburg, 2022), clustering of Pb into nanoparticles (Kusiak et al., 2015, 2023), mixing between two domains of different ages (Schoene, 2014 and references therein), and partial metamorphic recrystallization (e.g., Davis et al., 1968; Geisler et al., 2007; Hoskin and Black, 2002). Experimental evidence has shown that during the radioactive decay of U and Th, alpha recoil damage accumulates in the crystal lattice and can lead to interconnected pathways allowing for chemical disturbance leading to discordant U-Pb dates (Geisler et al., 2002, 2007; Salje et al., 1999; Trachenko et al., 2002). Thus, many geological processes are known to induce discordance, including the buildup of metamict domains inside zircon crystals (Nasdala et al., 1998), meteorite-impact induced shock effects (Moser et al., 2009, 2011), crystal-plastic deformation (Reddy et al., 2006), fluid induced dissolution-reprecipitation (Geisler et al., 2002, 2007), weathering processes (Andersen and Elburg, 2022; Pidgeon et al., 2016), pyrometamorphic heating (Ulusoy et al., 2019), and metamorphic

46 recrystallization and overgrowth that inherits radiogenic Pb during recrystallization (Mezger and
47 Krogstad, 1997; Schoene, 2014).
48
49 The analytical expression of discordance has long been utilized for understanding the events that
50 cause it, yielding lower intercept ages interpreted to be resetting/alteration events. This is typically
51 done using linear regressions (Davis, 1982; Vermeesch, 2021; York, 1968) through datasets that
52 fall along a single chord – meaning they have one single upper intercept event (often igneous or
53 metamorphic crystallization) and one single lower intercept event (caused by one of several
54 potential mechanisms, discussed above). Such an approach has yielded meaningful ages for a
55 variety of geological processes (Mezger and Krogstad, 1997; Moser et al., 2009, 2011; Schoene,
56 2014).
57
58 While most modern U-Pb studies aim to minimize discordance rather than use it (see Schoene,
59 2014, and references therein), there has been increasing focus on using discordant data to date
60 geological events, as discussed below. Sedimentary detrital zircon analyses present an opportunity
61 for dealing with discordance when compared to igneous and metamorphic zircon studies (e.g.,
62 Kirkland et al., 2017; Morris et al., 2015; Reimink et al., 2016). Because each detrital zircon in a
63 sediment shares the general post-depositional history with other detrital grains, discordant data
64 may be interpreted together. Without the constraint of a geological history, discordant U-Pb data
65 can be ambiguous or impossible to interpret. When dealing with sedimentary detrital zircon U-Pb
66 data, other assumptions may be drawn upon to related discordant zircon U-Pb data points to one
67 another, leveraging variable discordance to extract geologically meaningful age information from
68 the full population. One assumption that is shared by most studies investigating discordant detrital
69 zircon data is the assumption that zircons within a sedimentary rock might experience the same
70 geological events (fluid flow, metamorphism, etc.) that could variably affect the U-Pb systematics
71 of individual zircon grains to generate a spread of discordant data. This shared history, but with
72 variable imprints, can be very useful when attempting to infer geological events that may impose
73 discordance.
74
75 Several suites of studies have developed methods investigating discordant zircon U-Pb data. One
76 such suite relies on a comparison between discordant and concordant portions of detrital zircon
77 populations (Kirkland et al., 2017, 2020; Morris et al., 2015; Olierook et al., 2021), the so-called
78 "Concordant-Discordant Comparison" (Kirkland et al., 2017). This method requires a concordant
79 data population to serve as a comparator and then goes on to calculate an expected upper intercept
80 age distribution from discordant data points using a range of lower intercept ages. The calculated
81 upper intercept age distribution is then compared to the concordant data distribution (assumed to
82 be "true" distribution) using a K-S test or other 'similarity' metric, from which the most likely time
83 of discordance is then inferred. This method requires that concordant and discordant data subsets
84 be derived from very similar underlying populations, and that discordance-inducing processes
85 affect all populations of grains equally such that no biases are imparted on the discordant
86 population distributions. Statistical tests can then be used to evaluate the merits of this assumption.
87
88 Another approach (which is built upon in the present work), maps probability density from a given
89 dataset that falls along predefined chords in U-Pb space (Reimink et al., 2016). This results in a
90 'likelihood' map across a range of upper and lower intercept ages. This likelihood map can be
91 interrogated many ways, including evaluating upper intercept probability across a range of lower

intercepts, or the inverse. Additionally, discordant and concordant data points can be weighted to focus on discordant probability and suppress the effect of clusters of concordant data on the likelihood map. This method inherently incorporates analytical uncertainty by uniquely calculating the probability contributed to each data point to a given chord (Davis, 1982). Thus, uncertain data points contribute small probability densities to many chords, whereas highly precise data contribute large probability densities to fewer chords.

Additionally, discordant data generated by multi-phase mixing of growth zones have also been utilized to reconstruct upper intercept ages of core components in several ways. These methods simply recalculate upper intercept ages using a single lower intercept age, projected through discordant data. This is an output of the likelihood mapping discussed above (Reimink et al., 2016), and such a calculation has used when the a lower intercept likelihood peak is determined to be an igneous overgrowth event due to anataxis (Rasmussen et al., 2023). Additionally, an inverted CDC approach has been used when the rim growth ages are independently determined (Olierook et al., 2021), by reconstructing the upper intercept ages by using the mean of a data point and an the lower intercept age.

Other approaches to treat discordance provide mechanisms for assessing or filtering for discordant populations (Andersen and Elburg, 2022; Powerman et al., 2021; Vermeesch, 2021), and identifying Pb-loss specifically in igneous samples (Sharman and Malkowski, 2024). At times filtering of discordant data can result in a significant number of data being discarded, at times up to more than 60% of the total dataset (e.g., Clemens-Knott and Gevedon, 2023).

Despite the difficulty in linking the ages between individual discordant zircon in detrital sediments, one useful assumption can safely be applied: after the deposition of the sediment, all the zircon grains have a similar thermal and geological history. However, importantly, each grain will respond to these geologic events differently due to the unique crystallization, radiation damage, and previous thermal/annealing history of that particular grain. This shared history, but variable response, can be utilized to estimate ages of lower-temperature events than are typically recorded in zircon U-Pb ages (Kirkland et al., 2017; Morris et al., 2015; Reimink et al., 2016). We provide a robust analytical framework for determining the timing of these discordance-inducing events. We empirically show that detrital zircon grains from a sediment that was affected by contact metamorphism and fluid flow can be used to estimate the age of metamorphism and fluid alteration using zircon U-Pb discordance alone, without a significant concordant data fraction (c.f., Kirkland et al., 2017; Morris et al., 2015). Discordance is an undervalued and useful feature of detrital zircon populations, though more work is required to fully evaluate the applicability of the various frameworks that use discordance to date geological events.

2. Methods
2.1 Theoretical Framework
Here we date in situ alteration of detrital zircons based on the approach to discordance outlined by Reimink et al. (2016). In this framework, a numerical algorithm is used to calculate the probability distribution of a zircon U-Pb dataset across a range of synthetic discordia chords that represent candidate chords spanning a defined age range. Essentially, a 'mesh' of potential discordia chords is created at a defined interval (e.g., every 1 Ma a new chord is created) wherein each line has a unique upper and lower intercept age (Fig. 1b). Then, the total probability that falls on each chord

138 is calculated by determining the probability that each individual datapoint contributes to each
139 chord, using the equations of (Davis, 1982). The total probability is summed for each chord and
140 termed 'likelihood'. Further details on the method can be found in Reimink et al. (2016).

141

142 Reimink et al. (2016) discussed several different
143 normalization strategies to avoid biasing the
144 calculated probability distributions, including
145 homogenizing the uncertainty across a U-Pb dataset,
146 weighting against concordance (towards discordance),
147 and others. These normalizations can be useful to
148 prevent artificially biasing due to clusters of
149 concordant data, or biasing due to heteroscedastic data
150 (i.e., with non-uniform variance; Vermeesch, 2012). In
151 detrital zircon datasets, collected from rocks without
152 post-depositional disturbances, the chord with the
153 highest probability is likely to be associated with a
154 group of zircon crystals that have the same upper
155 intercept age, regardless of whether they are
156 discordant or not. In such an analysis, the upper
157 intercept ages are the most useful output. Thus, dating
158 a post-depositional discordance-inducing *lower-*
159 *intercept* event requires a different approach. The
160 present method modifies the original calculations to
161 determine the most likely lower intercept age across a
162 sample set that may have a range of upper intercept
163 ages. For example, using the Reimink et al. (2016)
164 calculation on a detrital sample which has a large
165 population of near-concordant grains at 1600 Ma and
166 experienced a Pb loss event at 30 Ma, the chord with
167 the highest probability would likely be chord between
168 30 and 1600 Ma (Fig. 1). However, 30 Ma lower
169 intercept ages associated with any other upper intercept
170 age would not be included in the probability of the 30
171 Ma lower intercept age, as only the 30−1600 Ma chord
172 is considered. If a detrital zircon population contains
173 grains that crystallized at 1000 Ma, 1200 Ma and 2700
174 Ma and these grains also experienced *in situ* Pb-loss at
175 30 Ma, that Pb-loss would go mostly undetected by the
176 previous method, though each upper intercept age
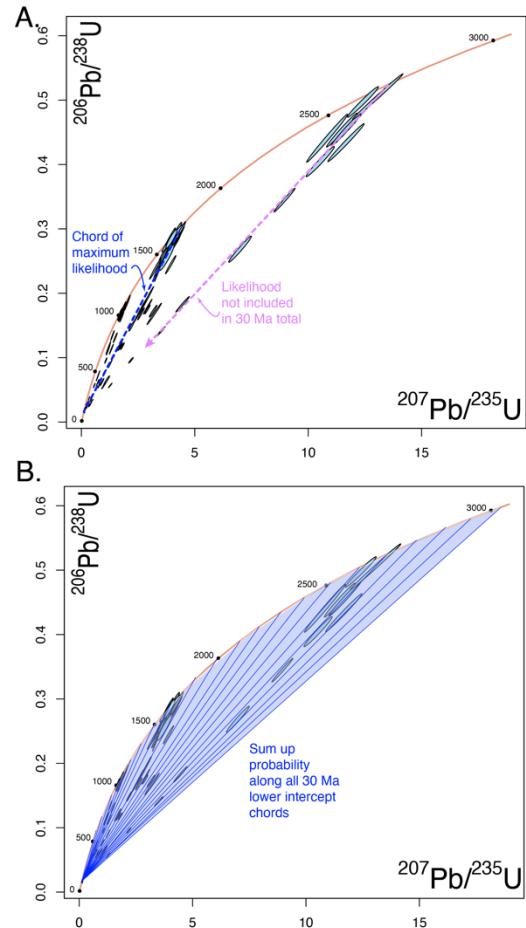177 would be resolved independently.

178

Figure 1: Example data showing why the sum probability density is required to accurately define likelihoods for lower intercept ages. In this synthetic dataset, there are many near-concordant ~1600 Ma datapoints. This cluster of near-concordant data will yield a higher probability for any chord anchored at 1600 Ma. A new method is required to evaluate the total probability contributed to any lower intercept age from a range of upper intercept ages. Panel B shows how the total probability density contributed to all lines with a 30 Ma lower intercept age could capture the likelihood of lower intercept ages in that window.

179 To rectify this issue, here we introduce a modification
180 to the original calculation. We add an additional step
181 that sums the total probability aggregated to each lower intercept age. Using the example above,
182 we add up all the probability accrued to all the lines with a lower intercept age of exactly 30 Ma.
183 Thus, the probability accumulated by the 30−1580 Ma chord would be added to the probability
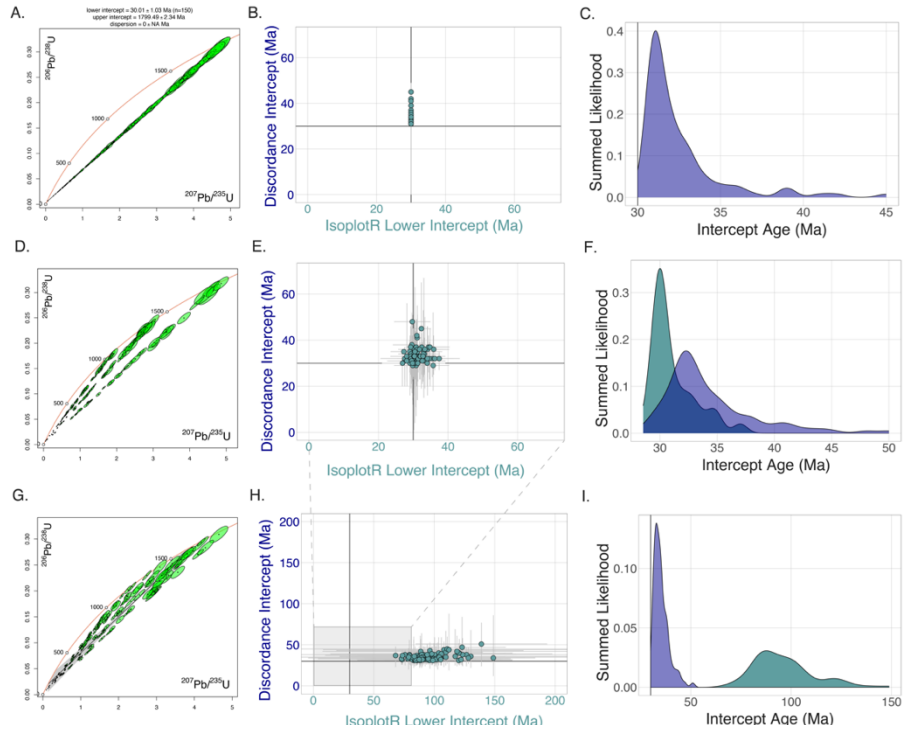
accumulated by the 30–1581 Ma chord, the 30–1582 Ma chord, etc. This sum is then divided by the number of chords that have a given lower intercept age to normalize across the age range of interest. This value is then termed 'summed likelihood' as it is a normalized value and no longer a probability density estimate. The results of this modeling approach theoretically return an estimate of the potential that a given lower intercept age may be a true post-depositional disturbance age, though it is normalized by the number of analyses and number of chords in any given model.

2.2 Benchmarking with Synthetic Datasets

To test the sensitivity and accuracy of our theoretical approach to extracting the ages of post-depositional discordance-inducing events from detrital zircons, we constructed several synthetic datasets and benchmarked our approach against single isochron regression techniques. We created synthetic data that aims to replicate aspects an actual zircon U-Pb dataset from Tintic formation detrital zircons (presented in Section 3). To do this, we used three categories of synthetic datasets (Fig. 2).

1. A U-Pb dataset that defines a perfect discordia line with an upper intercept of 1800 Ma a lower intercept of 30 Ma
2. A dataset with three upper intercept ages (1800 Ma, 1400 Ma, and 1100 Ma) all of which have discordance imposed at a shared lower intercept of 30 Ma
3. A dataset where each grain has an upper intercept age randomly selected from a range of ages (1800–1100 Ma) and all have a shared lower intercept of 30 Ma.

For each of the three categories, a synthetic data population was generated that contained 150 U-Pb data points. The number of datapoints was chosen as a typical number of analyses in detrital zircon datasets. However, see Section 2.3 for further discussion of this aspect. Each data point was randomly assigned an upper intercept and lower intercept age based on the model structure. In the case of the perfect line, all data points had the same upper intercept age. Then, each data point was assigned a random amount of discordance between 99.95% and 1%, selected from a flat

Figure 2: Input data and results from a synthetic data modeling procedure. Panels A, D, and G show examples of the synthetic input data, plotted on U-Pb concordia diagrams. The center panels (B, E, H) show the mean and uncertainties of the Isoplot R regression lower intercept age compared to the lower intercept values derived from the discordance modeling approach. Each data point represents a single synthetically generated dataset of 150 data points. The rightmost pane (C, F, I)l shows the distribution of lower intercept ages from each method with the blue curve representing the ages produced by the discordance model and the green curve representing the ages generated by the model 1 regression in IsoplotR. Note the change of scale in Panel H compared to E and B.

5

probability distribution. This random discordance accounts for the fact that each individual zircon grain, and indeed portions of grains, have differing resetting susceptibilities due to a variety of factors. The ratios of interest for each data point were assigned a random uncertainty value between 2–5% of their isotopic composition.

Each synthetic data set of 150 points was then evaluated in two ways. First, the traditional U-Pb regression ages were derived using the commonly used "York fit" approach (York, 1968) as implemented in IsoplotR (Vermeesch, 2018b), from which the upper and lower intercept ages were extracted. For the model constructed with three discrete upper intercept ages, we calculated three independent isochron regressions in IsoplotR, one for each population of synthetic data with a unique upper intercept age, and then calculated the weighted mean lower intercept age of these three regressions. Second, the data were input into our discordance modeling procedure and the maximum sum likelihood was extracted as well as the full width, half max of that peak – a measure of the spread in our modelled spectral data. This entire procedure was repeated 100 times for each of the three categories, resulting in 300 model runs.

The results from the outputs of the 'York fit' approach (model 1 regression in Isoplot R) are compared to our discordance modeling approach to benchmark the discordance dating procedure against well-accepted regression methods. Figure 2 shows the three different types of models, with the
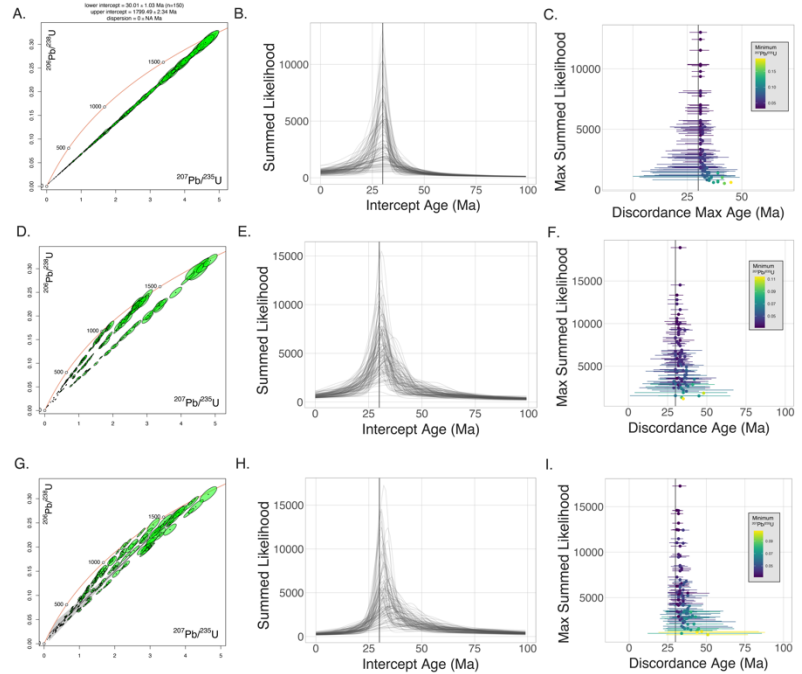

Figure 3: Results from the three sets of model runs for the discordance modeling procedure. The left panels show examples of the input datasets (same as Fig. 2). The central panels show lower intercept likelihood curves for the 100 model runs in each category of model. The right panels show the peak location, the uncertainties (derived by a full-width half-max calculation), and are colored according to the lower $^{207}Pb/^{235}U$ value in a given synthetic dataset. The discordance modeling procedure yields similar results independent of the input data type.

calculated lower and upper intercept ages from each synthetic dataset. Note that in Fig. 2C, the IsoplotR lower intercepts are tightly bound at 30 Ma so the probability density is not shown here. Figure 3 shows the discordance dating outputs in more detail, with individual age distributions shown from the discordance dating outputs.

The outputs of each calculation method are summarized in Fig. 4. For the simplest scenario, the perfect discordia line, the discordance dating model has larger uncertainties associated with the lower intercept age as compared to York-fit regressions. Note that in this version of the analysis, we are focusing on a small portion of the total U-Pb Discordia space, such that the area under each individual curve in Fig. 3C, F, and I are not all uniform. Sharp peaks are correlated to how close

276 the 'youngest' analysis is to the 30 Ma lower intercept, where precise lower intercept estimates are
277 typically derived from populations of data points that have some analyses close to the concordia
278 curve near the lower intercept age. It is expected – and observed (Fig. 4) – that the York fitting
279 procedure should outperform the discordance dating algorithm with respect to precision on the
280 lower intercept for the simplest case where
281 data can be regressed on a single line.
282 However, both methods still recover the
283 accurate lower intercept age within
284 uncertainty.
285
286 When considering more complex U-Pb
287 populations (for example the lower panels
288 in Fig. 4) that contain many primary (upper
289 intercept) U-Pb ages, the discordance
290 dating procedure expectedly outperforms
291 single linear regression and weighted
292 means of multiple linear regressions, as
293 used in Isoplot calculations. In the case of
294 having multiple discrete upper intercept
295 ages (middle panel in Fig. 4), the
296 discordance dating, although less precise,
297 provides improved accuracy and likely a
298 more reliable uncertainty estimate.
299
300 This is an expected result. A linear
301 regression method is obviously poorly
302 suited for highly scattered data that do not
303 share a common linear relationship.
304 Another method for extracting lower-
305 intercept age information, the
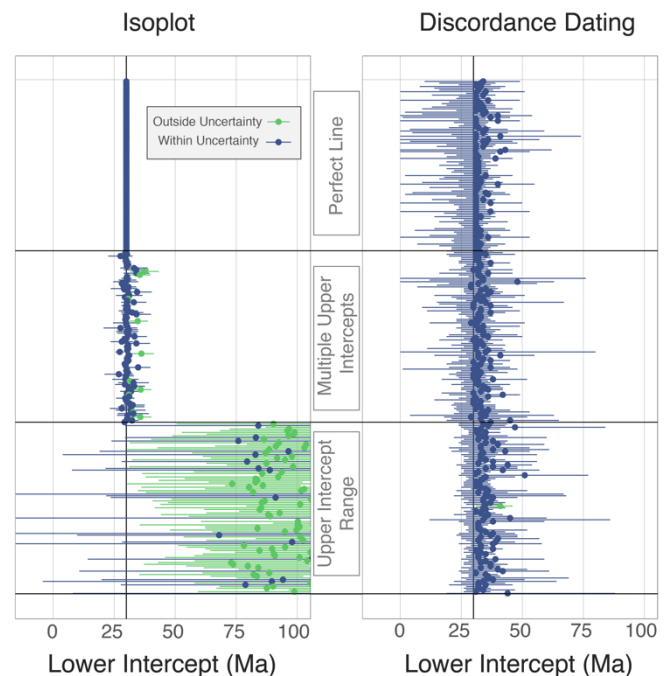306 Concordant-Discordant Comparison

Figure 4: A comparison of the lower intercept ages and uncertainties for the Isoplot regression calculations and the Discordance Dating method for all synthetic data runs. Each point is a unique dataset and the uncertainties are given for each regression point. The color of each point corresponds to whether the lower intercept age is within uncertainty of the pre-defined lower intercept of 30 Ma or not. The Discordance dating method provides more reliable results across a range of data types than simple linear regression models. d

307 method (Kirkland et al., 2017; Morris et al., 2015) requires a fraction of concordant data to use as
308 a comparator for refining a lower-age estimate. Due to this requirement, the CDC technique is not
309 expected to perform well in these synthetic datasets that have very little concordant data, and
310 indeed it does not perform well on the natural Tintic detrital zircon data discussed later (see Section
311 3.3).
312
313 This exercise also sets expectations for the uncertainties and potential biases on the lower intercept
314 that can be derived from this procedure. Focusing on the models with a range of upper intercept
315 ages, discordance dating returns a maximum uncertainty envelope that is on average ~20 Ma
316 (average peak width using FWHM on each peak). However, the central peak of the discordance
317 dating (the maximum likelihood lower intercept age) for these 100 models is 35 Ma +/- 6.8 Ma
318 (2SD), which may be a better uncertainty estimate for the discordance dating procedure (discussed
319 in Section 3.2 for natural data). The discordance dating procedure rarely returns peak centers that
320 are younger than 30 Ma, though it commonly returns peak centers older than 30 Ma. This bias to
321 older lower intercept ages is likely due to the sensitivity of the discordance dating procedure to the

position of the youngest point in any dataset – or the most 'reset' grain in any population. This is also important for our later interpretations – discordance dating is highly unlikely to return a maximum peak position that is too young (assuming no modern-aged discordance in the population), and any maximum peak position can likely be interpreted as a maximum age value for the true lower intercept resetting age.

2.3 Age Sensitivity and Precision

The underlying modeling approach used in this work fundamentally relies on an angular intersection between discordant data arrays and the 'concordia' curve in U-Pb space. Thus, due to the shorter half-life of the ^{235}U isotope system, this angularity will decrease as a function of the maximum age of the oldest zircons in any sample set. Put another way, older detrital zircon grains might be more likely to yield precise discordance dating lower intercept ages.

In an attempt to quantify the effect of older primary ages on discordance dating intercept age precision and provide guidance on the geological scenarios where discordance dating might provide useful chronological information, we conducted an additional suite of simulations that varied the primary age range of zircons in synthetic detrital zircon datasets. These simulations followed the methods for the datasets shown in Fig. 3G-I. We randomly selected a maximum upper intercept age between 100 Ma and 3500 Ma, then randomly selected a minimum upper intercept age that is older than 100 Ma, but younger than the maximum upper intercept age. We then followed the same steps outlined above, randomly generating datapoints with upper intercepts in that age range, randomly applying discordance, and then running the discordance dating methodd. We repeated this process 100 times with varying maximum and minimum upper intercept ages, all containing induced discordance at 30 Ma.

Results from this modeling exercise are somewhat non-intuitive (Fig. 5). Within the confines of the model parameters (an equal number of datapoints, homogeneous discordance distribution, random sampling, etc.) there is limited correlation between the precision in any discordance dating lower peak and the oldest age in a detrital zircon population (Fig. 5D). Much of the variation in discordance dating lower intercept ages seems to still be explained simply by the amount of discordance in the data – the more discordant the data the more precise any discordance dating result is likely to be (Fig. 5E). There does not appear to be a younger limit on the applicability of the discordance dating procedure, nor any obvious constraints on the upper age range of a detrital zircon dataset. In our synthetic models there is a similar range of peak distributions, a similar structure of the underlying likelihood distributions, and little excess imprecision induced by having younger grains in the sample. Thus, a geochronologist might hope to gain some degree of lower intercept age insight from the discordance dating method across a wide range of sample types, including samples with exclusively Phanerozoic detrital zircons.

However, this modeling reinforces the need for discordant data to produce reliable results. Thus, an optimal analytical campaign will intentionally analyze discordant portions of zircon grains that would be typically avoided in modern in situ analytical routines. Importantly, enough analyses are required, likely in the many dozens of discordant datapoints, to achieve a sufficient data density along meaningful discordia arrays.
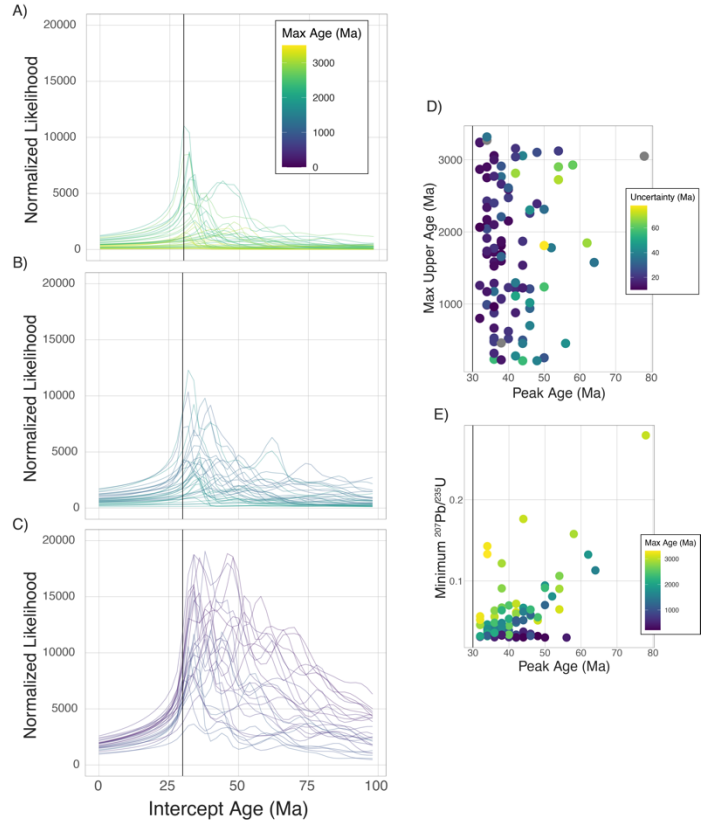

Figure 5: Results from synthetic models that varied the maximum primary age of the detrital zircon population, with maximum ages ranging from 3500 Ma to 200 Ma. Panels A, B, and C show the discordance dating outputs for datasets with maximum ages greater than 2 Ga, maximum ages between 1 and 2 Ga, and maximum ages below 1 Ga, respectively. Panel D shows the summary of the maximum lower intercept peak age plotted against the oldest upper intercept grains in the population, with little correlation between them. Panel E shows a general correlation between the minimum $^{207}Pb/^{235}U$ in the discordant dataset and the resulting discordance dating peak age, reaffirming the conclusion that the more discordant individual analyses are in a given dataset, the more accurate discordance dating can be.

3. Alta Stock Detrital Zircon Results

3.1 Methods and Results

To test the discordance dating strategy outlined above on natural samples with a known history, we conducted a laser ablation ICPMS analytical campaign targeting a well-studied metamorphic aureole with a known fluid-alteration history. We sampled a metasedimentary unit from the well-studied Alta stock metamorphic aureole, Utah (Brenner et al., 2021; Cook et al., 1997; Moore and

Kerrick, 1976; Stearns et al., 2020). The Alta stock intruded a suite of mid-Paleozoic sedimentary rocks in the late Paleogene (36–30 Ma; Stearns et al., 2020 and references therein) and was exposed through Miocene-aged uplift and titling along the Wasatch fault and Pleistocene glaciations and erosion in Little Cottonwood Canyon (Stearns et al., 2020 and references therein).

The Alta stock is one of a handful of plutons in the region that formed between ~36 Ma and ~30 Ma (Bromfield et al., 1977; Crittenden et al., 1973; Kowallis et al., 1990; Stearns et al., 2020). Titanite and zircon age constraints from the Alta stock indicate it was emplaced near the early stages of this interval (Crittenden et al., 1973; Stearns et al., 2020). Stock emplacement was accompanied by contact metamorphism in the host units and hydrothermal fluid alteration (Brenner et al., 2021; Cook et al., 1997; Moore and Kerrick, 1976). This fluid flow was primarily down-temperature and was focused on mixed carbonate-siliciclastic beds facilitated by porosity-forming decarbonation reactions (Cook et al., 1997). Previous geochronology on magmatic and overprinted zircon along with magmatic and metamorphic aureole titanite phases indicates Alta stock contact metamorphism extended from >30 to 25 Ma (Stearns et al., 2020). This, in combination with trace-element thermobarometry, led Stearns et al. (2020) to conclude that the earliest (36–30 Ma) phases were dominated by high temperature plutonism and metamorphism, whereas hydrothermal alteration activity remained active until ~23 Ma, particularly at the margins of the Alta stock.
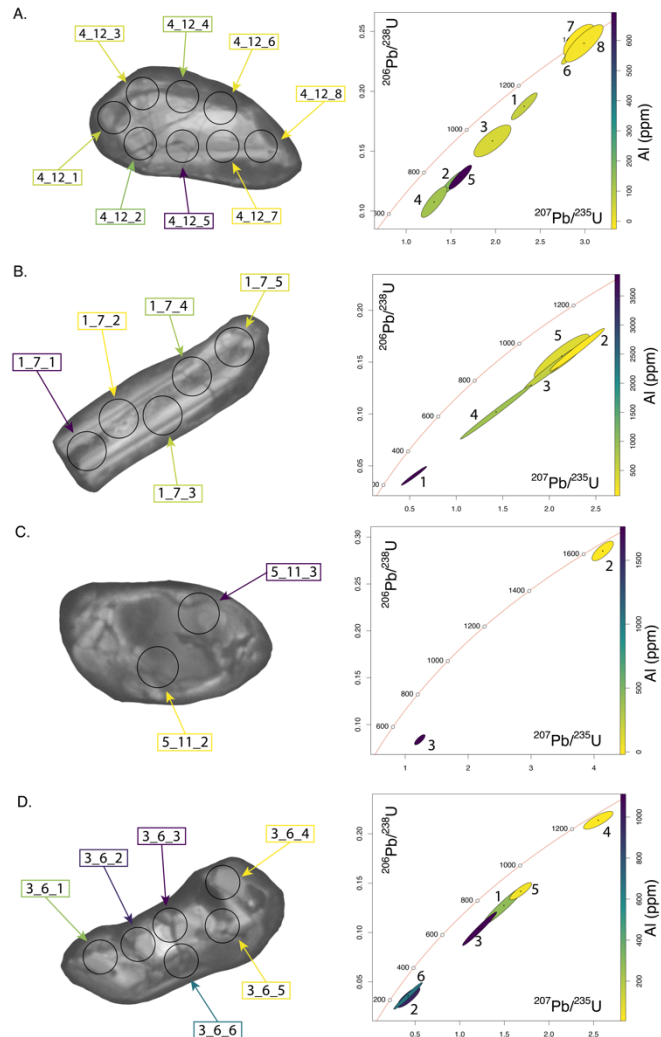

Figure 6: Representative Tintic detrital zircons and their U-Pb isotopic data. Each analysis point is labeled, where color labels correspond to the Al concentration of the analytical volume. The color scales vary between grains. Spot sizes are 30 μm in diameter.

We focused on a single sample of the Cambrian Tintic quartzite. This was collected ~200m from the contact with the Alta stock contact, above the tremolite-in isograd, and experienced metamorphic and fluid-alteration temperatures of ~450° C (Brenner et al., 2021; Cook et al., 1997). This metamorphic and alteration history, combined with the ages of detrital zircons found in the Tintic formation ranging from 1.0 Ga to <2.5 Ga (Matthews et al., 2017), provides an ideal testing ground for determining the accuracy and precision of the discordance dating technique.

Detrital zircons were isolated using standard crushing and mineral separation practices. Limited hand picking of zircons was conducted in an attempt to avoid biasing the results at that stage. Zircons were selected from other heavy minerals, but no preference was given for quality or morphology of zircon grains at this picking stage. Zircons were mounted in epoxy, polished to midsection, imaged using secondary electron imaging techniques, and subsequently analyzed by laser ablation techniques following the methods of (Cipar et al., 2020; Schoonover et al., 2024). A Teledyne/Photon Machines Analyte G2 excimer laser was used, with a Helex2 ablation cell, for all laser ablation work.

Zircon U-Pb and trace element data was collected in three sessions from Feb. 2023 to May 2023. Two sessions, on Feb. 28th, 2023 and March 3rd, 2023, collected U-Pb-TE on the Thermo Scientific iCapRQ quadrupole mass spectrometer in the LionChron analytical facility. Isotopes measured included ^{27}Al, ^{29}Si, ^{44}Ca, ^{51}V, ^{57}Fe, ^{146}Nd, ^{147}Sm, ^{163}Dy, ^{172}Yb, ^{204}Pb, ^{206}Pb, ^{207}Pb, ^{232}Th, and ^{238}U. The analytical session on May 30th, 2023 utilized split stream techniques, where ^{204}Pb, ^{206}Pb, ^{207}Pb, ^{232}Th, ^{235}U and ^{238}U were analyzed on the Thermo Scientific Element XR ICPMS system and ^{7}Li, ^{23}Na, ^{27}Al, ^{29}Si, ^{31}P, ^{43}Ca, ^{45}Sc, ^{49}Ti, ^{55}Mn, ^{57}Fe, ^{59}Co, ^{60}Ni, ^{85}Rb, ^{88}Sr, ^{89}Y, ^{90}Zr, ^{93}Nb, ^{119}Sn, ^{133}Cs, ^{137}Ba, ^{139}La, ^{140}Ce, ^{141}Pr, ^{146}Nd, ^{147}Sm, ^{153}Eu, ^{157}Gd, ^{159}Tb, ^{163}Dy, ^{165}Ho, ^{166}Er, ^{169}Tm, ^{172}Yb, ^{175}Lu, ^{180}Hf, and ^{182}W were measured on the iCapRQ quadrupole mass spectrometer. ^{235}U was calculated from ^{238}U and the U-isotopic composition of 137.818 (Hiess et al., 2012) due to low ^{235}U signals. NIST SRM 612 glass was used as a trace-element primary reference material and zircon 91500 was used as a primary reference material for U-Pb isotopic measurements. Uranium-lead and trace element data was filtered, standardized, and normalized using the Iolite data reduction software.

Resulting U-Pb isotopic data for zircon reference materials shows good agreement with accepted values across all three analytical sessions (see "ZirconRM_UPbCompilation.png" in the online repository). The resulting ^{206}Pb/^{238}U ages generally within uncertainty of the accepted values, apart from: GJ-1 from Sessions #2 and #3 (~3% too low), and Peixe from Session #1 (~3 % too high). However the results are accurate enough for the purposes of this study, which relies on U/Pb variation in across a much larger range of U-Pb space.

Trace element data from the zircon reference materials similarly shows consistency within the documented range of trace element concentrations in zircon reference materials (see "ZirconTE_Supplementary.pdf" in the online repository). For instance, the Al concentrations in GJ-1 are nearly identical to published values, with a mean of 3.8 compared to an accepted value of 3.75 ppm (Caulfield et al., 2025). Importantly, though the Al concentration in some reference materials are well characterized (Caulfield et al., 2025), other elements typically used as indicators of alteration (Ca, Fe) are not. Even within a well-studied reference material such as 91500, Al concentrations vary substantially intra- and inter-grain. Though some of our reference material trace-element concentrations are accurate, the concentrations of Al, Ca, and Fe may not be. However, we have chosen to include the concentrations of these alteration elements in our data tables to give the reader a rough estimate of the expected concentrations in altered zircon domains. Further work on the chemical implications of alteration is needed to help characterize the various potential causes of discordance, and we hope that broad estimates of the concentrations of such elements in altered zircon grains can help guide such future work.

Secondary zircon reference materials include Peixe, GJ-1, Plesovice, and MudTank. Secondary reference material U-Pb results are shown in the supplements. The only session where a secondary reference material's U-Pb age was > 2% outside of the accepted age was in the March 3rd session, where GJ-1 had an average ^{206}Pb/^{238}U age ~3% lower than the accepted age. However, during the same session Peixe returned a ^{206}Pb/^{238}U age in line with the accepted age. Position-dependent fractionation may have played a role in the slightly increased inaccuracy of the GJ-1 zircon during this analytical session. All other sessions returned secondary reference material results within 2% of the accepted ages (see supplementary materials for data and results).
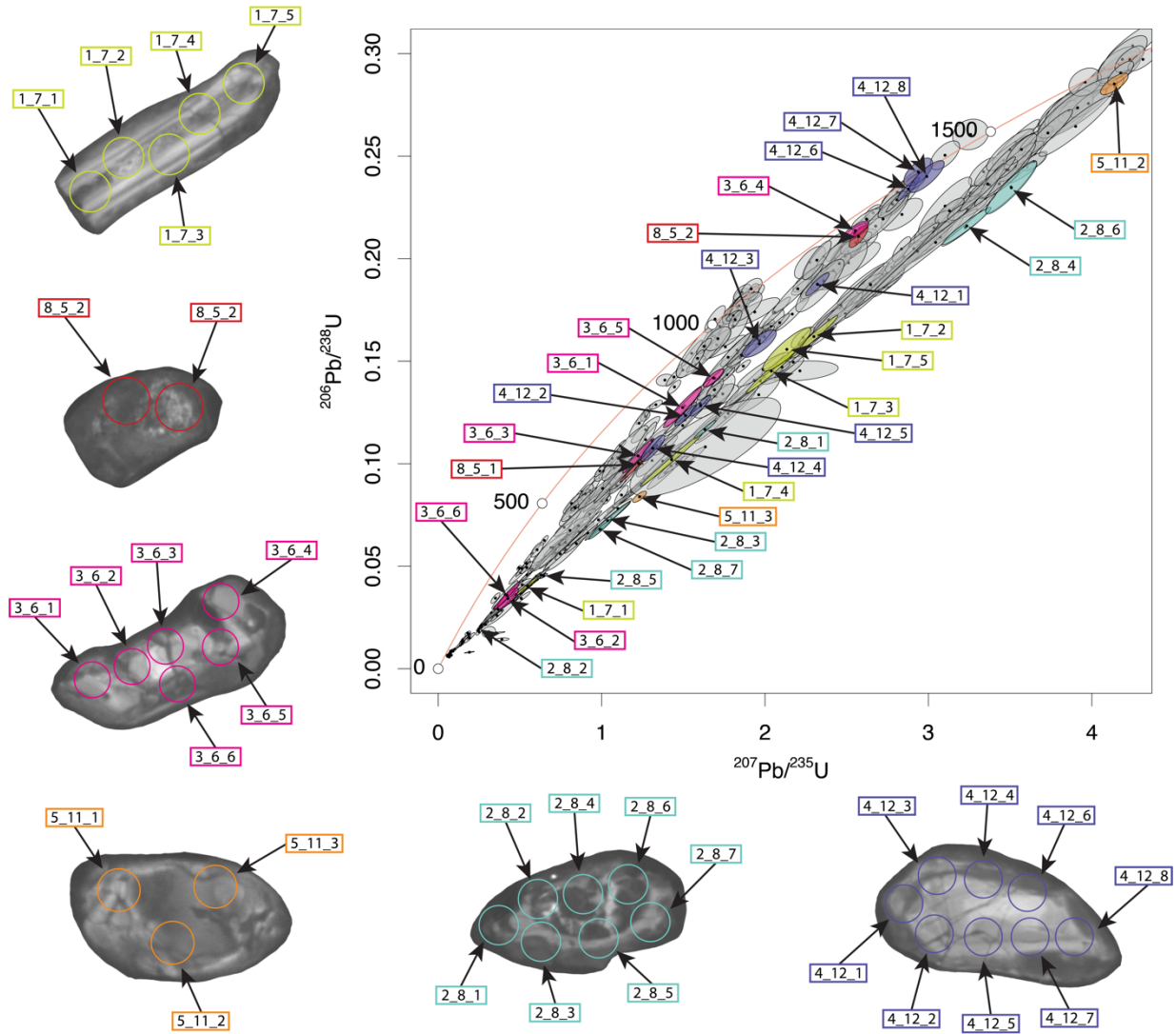
Figure 7: U-Pb data from detrital zircons extracted from the Tintic quartzite sample studied in this work. Zircon secondary electron microscope images are shown with spot locations correlated to individual data points. For scale, laser spots are all 30 μm.

Detrital zircons from the Tintic formation show a wide range of igneous and metamorphic/fluid alteration textures. Many (Fig. 6a,b) contain internal zones with apparent oscillatory zoning while others (Fig. 6a,c,d) show clear metamorphic rims along with wispy internal disturbance textures

495 (Corfu, 2003). While the full dataset contains a wide range of U-Pb isotopic discordance (Fig. 7),
496 individual grains can often display a wide range of internal age and chemical variability (Figs.
497 6,7).
498
499 Zircons from this sample show a range of ^{207}Pb/^{206}Pb ages between 1 Ga and 1.8 Ga, and a wide
500 range in ^{206}Pb/^{238}U ages (Figs. 6,7), leading to a large spread in the associated discordance. In
501 typical detrital zircon work, where filtering for concordance is normal (e.g., Gehrels, 2014), the
502 vast majority of these analyses would be filtered out and not considered further. The U-Pb data
503 were used as inputs into the updated version of the discordance modeling algorithm of Reimink et
504 al. (2016). The results of modeling are shown in Fig. 8. As discussed previously, the discordance
505 modeling produces a 'sum likelihood' value across a range of lower intercept ages, in this case
506 from 0 to 50 Ma. Note that the lower intercept range is independent of the model outputs as the
507 data reduction is conducted geometrically. The most likely lower intercept age is definitively
508 greater than 0 Ma, as the model is capable of modeling future ages and likelihood declines rapidly
509 prior to 0 Ma. The peak in likelihood is ~24 Ma, and sensitivity tests (Section 3.2) show that the
510 best fit age is 16–28 Ma, based on the locations of the bootstrap-resampled sensitivity data (Section
511 3.2).

3.2 Uncertainty Analysis

In order to test the sensitivity of the results shown in Fig. 8 to individual data points or groups of data points and conduct uncertainty analysis, we conducted a bootstrapped resampled modeling routine. The full Tintic Formation dataset was resampled with a pick-and-replace method to create 1000 synthetic datasets that contained the same number of data points as the original dataset (407 analyses). Each of these synthetic datasets was put through the discordance dating method and summed likelihood lower intercept ages were calculated. The maximum summed likelihood values and the ages of those maximum values were aggregated for each synthetic dataset. Figure 8B shows the distribution of the 1000 resampled discordance models, the majority of which have lower intercept peaks that cluster between 18 and 28 Ma. These ages are centered on the youngest ages documented by Stearns et al. (2020) from endoskarn titanites with ages down to 23 Ma which have been found in the Alta Stock metamorphic halo. Our data show that discordance induced by metamorphic resetting and/or fluid induced Pb-loss at this time affected a large portion of detrital zircons in the Tintic formation and validates our theoretical approach to discordance dating of disturbances in detrital zircons.

Non-radiogenic Pb, termed 'common lead', can be found in meaningful concentrations in zircon, particularly metamorphic or otherwise perturbed zircon crystal lattices (e.g., Andersen, 2002; Schoene, 2014). The correction of this common Pb is necessary for accurate and precise geochronology, and several algorithms can be applied to remove the effect of common Pb from the U-Pb age calculations. The Tintic formation detrital zircon analyses do contain some common Pb, with higher concentrations present in a fraction of the more discordant analyses. To test if common Pb corrections influence our discordance dating methodology, we analyzed the Tintic formation zircons after two different common Pb correction types, in addition to the uncorrected data shown in Fig. 8 (green line in A). These results are shown in Figure 9. First, we apply various
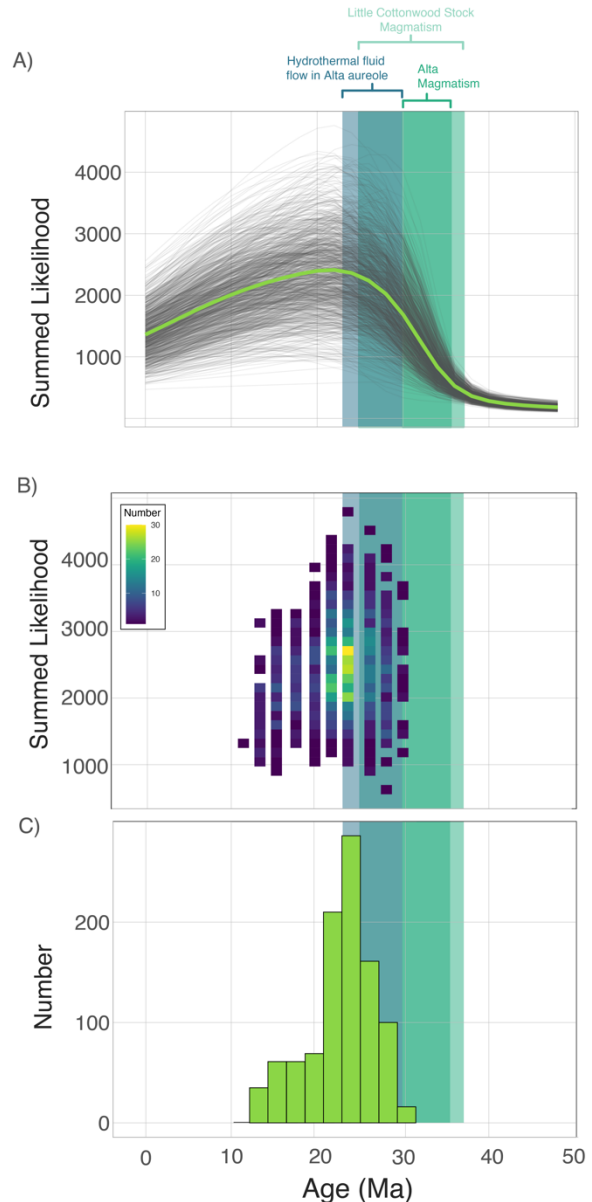

Figure 8: Outputs from discordance dating of Tintic formation zircons, and bootstrapped resampling efforts. A shows the summed likelihood lower intercept results of discordance dating. B shows the age and maximum sum likelihood value for each maximum value calculated from the curves shown in A. C shows a histogram of the peak positions in Ma. The discordance dating age can be estimated based on the resampling method to be 24 +4/-8 Ma based on the location of the median, 5th, and 95th percentile peak locations shown in C.

common Pb correction methods to subtract the contribution of 'common Pb' to the ^{206}Pb and ^{207}Pb signals. One common method (e.g., Schoene, 2014) is to use the ^{204}Pb signal as an indication of the amount of common Pb, assume a Pb isotope composition using the Stacey-Kramers (Stacey and Kramers, 1975) global Pb-isotope evolution model, and subtract this common ^{206,207}Pb from the presumably radiogenic portion of the Pb. Another method involves the iterative solution to a series of equations assuming that the U/Th has not been disturbed and any time of Pb-loss is known (Andersen, 2002) – the latter assumption makes the method inappropriate for use with highly discordant data where the age of isotopic disturbance is unknown, data similar to the Tintic data evaluated here. Nevertheless, we show that there is little difference between the outputs of our discordance dating model on U-Pb data corrected using different common Pb
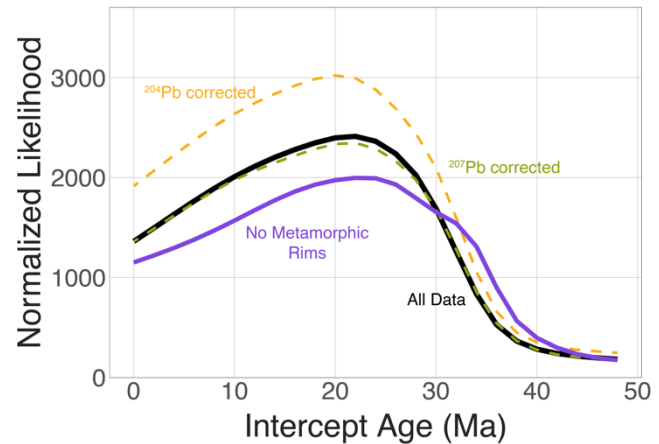

Figure 9: Plot showing the summed lower likelihood for Sample 2 U-Pb data with various common-Pb corrections applied. The black curves shows the base data with no common Pb correction. The orange curve shows the same data with a ^{204}Pb and Stacey-Kramers common Pb correction applied. The green curve shows the ^{207}Pb or Anderson correction applied to the same data. The purple line shows the lower intercept result for data that excludes all analyses that included a metamorphic rim growth feature. There is little change in the peak position across these various datasets, indicating that common Pb is unlikely to be affecting our results.

calculations (Fig. 9), suggesting that the discordance dating lower intercept age is robust from the influence of common Pb, at least for the Tintic Formation zircon dataset evaluated here.

Finally, uncertainty in the decay constants of ^{238}U and ^{235}U (Jaffey et al., 1971) may impact the discordance dating procedure to various degrees depending upon the age range of the zircon U-Pb data. Our discordance dating process fundamentally maps isotopic probability across Pb/U space, thus is not strictly dependent upon the decay constant uncertainties. Additionally, decay constant uncertainties are systematic uncertainties – meaning they apply to all data equally. In other words, if the 'true' ^{235}U decay constant is lower than measured by some degree, it will always be lower to that same degree. We can therefore perform a conservative assessment of the potential impact of uncertainty in the decay constants of the U isotopes by re-running the discordance dating procedure and simply changing the decay constants within uncertainty. In effect, this serves to shift the equal-age concordia line one direction or another in Pb/U isotope space, which changes the location of the age-ratio intercepts. For the Tintic formation zircon data, we can model the extreme examples of decay constant uncertainty by lowering the ^{238}U decay constant by 0.107% and increasing the ^{235}U decay constant by 0.137% (Jaffey et al., 1971), running the discordance dating procedure, then rerunning by raising the ^{238}U decay constant and lowering the ^{235}U decay constant. For the Tintic formation detrital zircon data, there is no change in the peak position of the lower intercept summed likelihood metrics, indicating that decay constant uncertainty does not impact the results of this study. However, decay constant uncertainty can affect interpretations of zircon populations that have significantly older discordance on the order of half a percent of the age. We have implemented a switch in the codebase allowing users to perform this uncertainty evaluation on their own datasets, but must note that this test may result in an unrealistically high estimate of

603 decay constant uncertainty as it does not take into account any correlation in the decay constant
604 errors that may exist (e.g., Mattinson, 2010).
605
606 At the current time, definitively distinguishing between the various types of isotopic disturbance
607 and resetting processes is not possible. However, differentiation could be done by, for instance,
608 combining zircon U-Pb-TE data with Raman spectrometer analyses of altered domains that could
609 quantify the crystallinity of the zircon lattice (Anderson et al., 2020; Nasdala et al., 2010; Resentini
610 et al., 2020; Zhang et al., 2000) and help determine which of these two models, metamorphic
611 recrystallization and/or fluid-induced Pb loss, was a dominant Pb-loss-inducing process in the
612 Tintic zircon population. However, this would need to be accomplished prior to destructive
613 analyses for U-Pb-TE via laser ablation. Addressing the micro-scale causes of U-Pb discordance
614 in detrital zircons will be important for evaluating the range of geologic settings where discordance
615 dating could be reliably applied to the rock record.
616
617 *3.3 Comparison with other discordance dating approaches*
618 The Concordant-Discordant Comparison method uses an approach that inverts discordant U-Pb
619 data using various lower-intercept ages, then compares the reconstructed upper intercept age
620 results to the concordant populations of the same sample (Kirkland et al., 2017; Morris et al., 2015)
621 to find the most likely lower intercept age. Here, we test the CDC method on the Tintic formation
622 U-Pb population and briefly discuss the outputs.
623 Figure 10 shows the results of the CDC method conducted on the Alta aureole Tintic detrital zircon
624 analyses. It is important to note that a small fraction (71 out of 407) of Tintic zircon analyses are
625 within 10% of concordance, so given the CDC method's reliance on a concordant fraction of data,
626 we should not expect this method to perform optimally. Figure 10A shows a comparison of the
627 CDC method to the discordance dating approach outlined in this work. The CDC method uses a
628 K-S statistic to compare reconstructed discordant populations with the concordant data, and the K-
629 S statistic returns low (near-zero) values for datasets that compare well to one another. In Fig. 10A,
630 we have inverted this K-S statistic such that high values (near one) represent data populations that
631 are more like one another. We have also normalized the discordance dating summed likelihood
632 metric to the maximum value (peak at 24 Ma), strictly for the purposes of comparison.
633

As shown in Figure 10A, the CDC method does not return peaks in the relevant statistic near 25-30 Ma for reasonable discordance cutoffs (10-20%), and only returns small, broad peaks in this time interval when the discordance cutoff is high (>30%). These results might suggest that the CDC method is highly sensitive to the fraction of concordant data present in any given sample and shows that resolving lower intercept ages without reliable concordant data, as in the case of the Tintic detrital sample analyzed here, is difficult.

However, a dearth of concordant data may not fully explain the lack of resolvability when using the CDC method. Figure 10B shows kernel density estimators for a wide range of reconstructed upper intercepts (all using a 15 Ma bandwidth, chosen for clarity). The red line shows the age of the 10% concordant data from the Tintic formation, which is used by the CDC method as the comparator and assumed to be the 'true' distribution. The colored lines are reconstructions of the discordant data fraction, colored by the age of the lower intercept used for the upper age reconstruction. The bold blue line shows the reconstructed upper ages calculated using a 24 Ma lower intercept age. The reconstructed upper ages calculated using a 24 Ma lower intercept age do have age peaks that match the peak locations of the concordant data (red line), however as shown
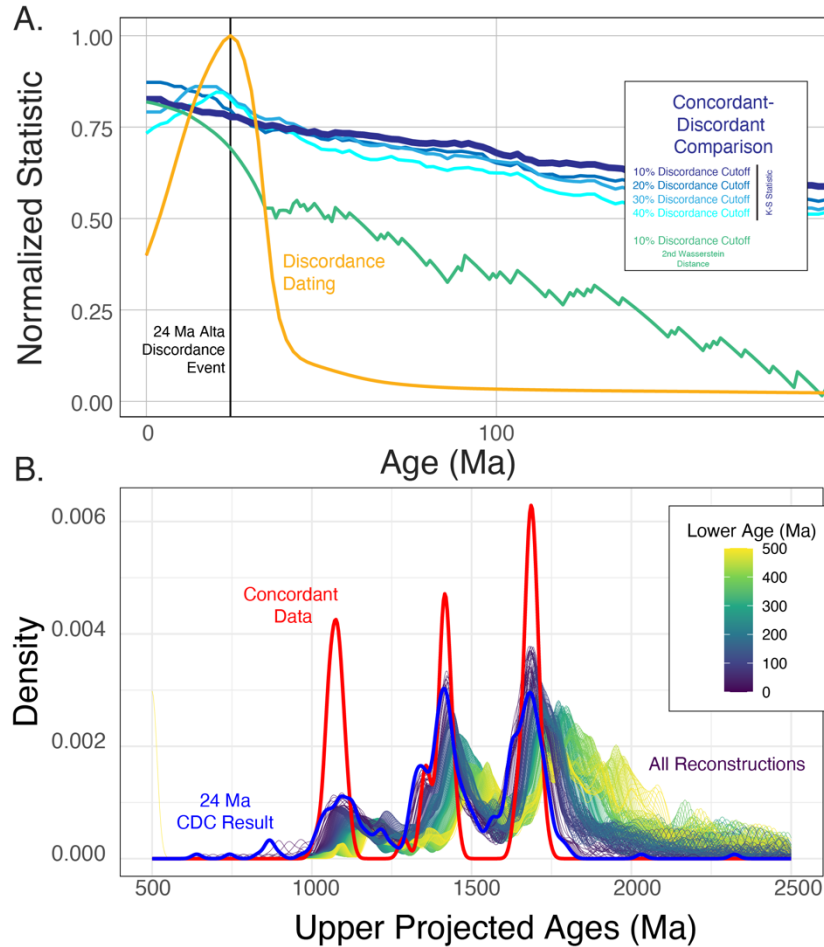

Figure 10: The Concordant-Discordant Comparison method applied to the Alta Tintic detrital zircon data. Panel A shows a normalized discordance dating result (normalized to the peak summed likelihood at 24 Ma), compared with the results of five different CDC model runs. Each run uses a different discordance cutoff for determining the concordant and discordant populations (10%, 20%, 30% and 40%). Note that we have inverted the K-S statistic and normalized + inverted the Wasserstein metric such that similar datasets will have a value closer to 1, again for comparison's sake. Panel B shows raw outputs from the CDC method across a wide range of ages. The red curve shows the 10% concordant data distribution. The colored curves show reconstructed upper intercept age distributions colored by the age of lower intercept used for the reconstruction. The bold blue labeled line shows the reconstruction using a 24 Ma lower intercept. Reconstructions are created using lower intercepts every 2 Ma from 0 to 500 Ma. Reconstructed peak locations match well for the 24 Ma lower intercept reconstruction, but the relative peak heights are significantly different, suggesting the K-S metric, which relies on a cumulative density plot comparison, is unlikely to give reliable comparison metrics.

679 in Fig. 10A, the K-S comparison statistic does not return this lower intercept age as a likely time
680 of discordance, except for minor, <24 Ma peaks when using very high (>30 %) discordance filters.
681
682 This suggests that part of the reason for the lack of lower intercept age resolution for the Tintic
683 formation detrital zircon data returned by the CDC test might be due to the comparison test statistic
684 itself. The K-S statistic returns the maximum vertical difference between two cumulative
685 distribution curves (Massey, 1951) such that 0 is a perfect match. The reliance of this statistic on
686 cumulative distributions means that the K-S metric is sensitive not only peak locations, but also to
687 relative peak heights. The dependence on relative peak heights is by design, and often implemented
688 in detrital zircon comparison statistics, as the relative proportion of grains of specific ages can be
689 of importance for detrital zircon geochronologists. Thus, most comparison statistics applied to
690 detrital zircon datasets are designed to also evaluate peak height differences (see the excellent
691 overview provided in Vermeesch, 2018b), and even the Wasserstein distance metric (Lipp and
692 Vermeesch, 2023) does not identify a 24 Ma peak when relying on a comparison to concordant
693 data filtered at the 10% level. It is possible that the use of comparison statistical tests may be
694 limiting the use of the CDC method for the Tintic zircon data presented here (Fig. 10B), which
695 experienced a discrete overprinting event ca. 30-24 Ma. For instance, the 1.1 Ga reconstructed
696 peaks are far lower than the 'concordant' data peak at that same time, while the 1.8 Ga
697 reconstructed peak is relatively high. This is likely causing the K-S statistical test (and other
698 similarity/dissimilarity metrics) to break down for this particular use case.
699
700 When dealing with discordance inducing events, biases may be imparted onto the discordant data
701 population due to various factors. We speculate that the Tintic 1.8 Ga detrital zircons, being older,
702 likely accumulated more radiation damage to the crystal lattice than the 1.1 Ga detrital grains.
703 Thus, during a 24 Ma alteration event, the 1.8 Ga population may have experienced more
704 disturbance, leading to more discordant data. This scenario would impart a dramatic bias in any
705 statistical comparison between the discordant and concordant data that relies on cumulative density
706 curves (e.g., K-S test, Wasserstein distance, etc.). As shown in Fig. 10B, the reconstructed upper
707 age distribution using a lower age of 24 Ma does indeed reproduce the peak locations well, though
708 not the relative peak heights. Further testing outside the scope of the present work is required to
709 fully evaluate the real-world applicability of various discordant data treatment approaches, where
710 they perform well and where they may break down.
711
712
713 **4. Outlook and Future Directions:**
714 Here we have showed that discordance dating may be used to date discordance-inducing events
715 that affected detrital zircon populations. We have shown that this method provides several million-
716 year age resolution on alteration events in rocks that experienced ~24 Ma fluid flow and
717 metamorphism at temperatures that reached ~450 °C. The high temperatures of metamorphism
718 within the Tintic formation sample may lead to the perception that discordance dating is a tool that
719 is applicable to high-T metamorphic settings only. However, several pieces of data suggest that
720 discordance dating may be an impactful method with wider applicability.
721
722 First, most zircon geochronologists pursue readily interpretable and therefore concordant data.
723 Geochronologists tend to select spots targeting regions of high zircon quality and pick laser or ion
724 probe analytical locations that are likely to retain a closed U-Pb system – a single metamorphic

growth rim or a single domain of clearly igneous zircon. Additionally, what little discordant data may have been collected in laboratories around the world is commonly filtered based on a discordance threshold. Thus, there is no clear way to determine the general prevalence of discordant data in detrital zircon datasets. Additional analytical focus on discordant grain volumes may lead to additional insight into the value of discordant data for geochronological purposes.

Second, discordance dating will theoretically become more precise if discordant grains have older initial crystallization ages and the resetting event is relatively young. Due to the geometry of U-Pb isotope space, older grains experiencing more recent discordance-inducing geological events will provide a more precise estimate of lower intercept ages. However, though the Tintic formation contains grains with primary ages up to ~1.8 Ga, other more ancient grains would provide additional precision to any discordance dating analysis. The larger the age dispersion in detrital zircon crystallization ages, the more precision discordance dating would yield for Phanerozoic alteration events. Thus, a sediment that experienced less aggressive fluid flow or metamorphism, but that had older detrital zircon grains, may yield important lower intercept age information, with uncertainties on the order of a few million years.

Third, there is a growing body of evidence that discordance in zircon can be induced in a wide variety of low-temperature environments. Both experimental (Geisler et al., 2001; Pidgeon et al., 1966) and empirical (Geisler et al., 2002; Morris et al., 2015; Pidgeon et al., 2016; Zi et al., 2022) studies have documented large degrees, and sometimes near total, discordance at much lower temperatures (100–200 C) than the Tintic formation zircons analyzed in this work experienced. Thus, it is possible that many suites of detrital zircons experienced low-T hydrothermal fluid flow events that induced Pb-loss and/or recrystallization to such a degree that discordance dating could provide useful age information.

Such information could prove useful when paired with other low-temperature chronometers dating such events as diagenetic xenotime growth (McNaughton et al., 1999), zircon cooling below 200-400 °C using Raman dating (Härtel et al., 2021), and U-Pb/U-Th-He double dating to derive low-T geological histories of individual grains. It is important to note that Raman dating and U-Th-He dating of zircon are both temperature sensitive phenomenon that would ideally target pristine zircon growth zones, whereas discordance dating requires analyses of damaged, discordant grains. The result is that these various techniques could be applied to the same grains within a given population to both extract detailed thermo-chemical histories, as well as intercalibrate the various dating techniques. Notably, more work is required to robustly determine the sensitivity of discordance dating to both fluid alteration and elevated temperatures. Such information will provide insight into the interplay between different low-T geochronometers applied to detrital zircons. Discordance dating may be particularly interesting as there are a limited number of geochronometers that are currently available to date reactive fluid flow events (brine migration, mineralizing fluid flow, low-T metamorphism, etc.) in sedimentary rocks– even imprecise age information is useful in such scenarios.

771
772 **5. Conclusions:**
773 We have documented a new tool for geochronologists to date in situ detrital zircon discordance-
774 inducing events. We have shown the utility of this technique using synthetic datasets and ground-
775 truthing by analyzing zircons within the well-studied Alta Stock metamorphic aureole. The
776 discordance dating technique returns discordance ages of ~24 Ma, which is the expected age of
777 fluid flow in this region. Our method may have significant applications to determining rates and
778 absolute dates of diverse geologic phenomena; basin brine migration, mineralizing fluid flow, and
779 low-grade burial metamorphism are just a few of the processes that may induce discordance in
780 zircon analytical volumes such that it is amenable to discordance dating.
781
782
783

Data Availability:
The data reduction code and raw data used for discordance modeling is available here: https://github.com/jreimink-isotope-geochem/discordance-dating and at the following Zenodo DOI 10.5281/zenodo.13972610
and a public-facing easy-to-use Shiny app is available here:
https://discordance.geosc.psu.edu/discordance_app/

Competing Interests:
The authors declare that they have no conflict of interest.

Author Contributions:
JR, JD, and ML conceived the study. AS carried out sample collection. RB, ES, AC, and JG separated zircons, collected U-Pb-TE data, and produced final results. JR and JD carried out modeling and sensitivity testing. All authors contributed to final data interpretation and manuscript production.

References:

Andersen, T.: Correction of common lead in U–Pb analyses that do not report 204Pb, Chemical Geology, 192, 59 79, https://doi.org/10.1016/s0009-2541(02)00195-x, 2002.

Andersen, T. and Elburg, M. A.: Open-system behaviour of detrital zircon during weathering: an example from the Palaeoproterozoic Pretoria Group, South Africa, Geological Magazine, 159, 561–576, https://doi.org/10.1017/S001675682100114X, 2022.

Anderson, A. J., Hanchar, J. M., Hodges, K. V., and van Soest, M. C.: Mapping radiation damage zoning in zircon using Raman spectroscopy: Implications for zircon chronology, Chemical Geology, 538, 119494, https://doi.org/10.1016/j.chemgeo.2020.119494, 2020.

Brenner, D. C., Passey, B. H., Holder, R. M., and Viete, D. R.: Clumped-Isotope Geothermometry and Carbonate U–Pb Geochronology of the Alta Stock Metamorphic Aureole, Utah, USA: Insights on the Kinetics of Metamorphism in Carbonates, Geochemistry, Geophysics, Geosystems, 22, e2020GC009238, https://doi.org/10.1029/2020GC009238, 2021.

Bromfield, C. S., Erickson, A. J., Haddadin, M. A., and Mehnert, H. H.: Potassium-argon ages of intrusion, extrusion, and associated ore deposits, Park City mining district, Utah, Economic Geology, 72, 837–848, https://doi.org/10.2113/gsecongeo.72.5.837, 1977.

Caulfield, J. T., Allen, C. M., Ubide, T., Nguyen, A., and Cathey, H. E.: Compositional heterogeneity in 91500, GJ-1/89 and TEMORA-2 zircon reference materials, Chemical Geology, 674, 122580, https://doi.org/10.1016/j.chemgeo.2024.122580, 2025.

Cipar, J. H., Garber, J. M., Kylander-Clark, A. R. C., and Smye, A. J.: Active crustal differentiation beneath the Rio Grande Rift, Nat. Geosci., 13, 758–763, https://doi.org/10.1038/s41561-020-0640-z, 2020.

Clemens-Knott, D. and Gevedon, M.: Using discordant U-Pb zircon data to re-evaluate the El Paso terrane: Late Paleozoic tectonomagmatic evolution of east-central California (USA) and intense hydrothermal activity in the Jurassic Sierra Nevada arc, Geosphere, 19, 531–557, https://doi.org/10.1130/GES02547.1, 2023.

Cook, S. J., Bowman, J. R., and Forster, C. B.: Contact metamorphism surrounding the Alta Stock; finite element model simulation of heat- and 18 O/ 16 O mass-transport during prograde metamorphism, American Journal of Science, 297, 1–55, https://doi.org/10.2475/ajs.297.1.1, 1997.

Corfu, F.: Atlas of Zircon Textures, Reviews in mineralogy and geochemistry, 53, 469 500, https://doi.org/10.2113/0530469, 2003.

Crittenden, M., Stuckless, J., Kistler, R., and Stern, T.: Radiometric dating of intrusive rocks in the Cottonwood area, Utah | U.S. Geological Survey, Journal of Research of the US Geological Survey, 1, 173–178, 1973.

843 Davis, D. W.: Optimum linear regression and error estimation applied to U-Pb data, Canadian
844 Journal of Earth Sciences, 19, 2141 2149, https://doi.org/10.1139/e82-188, 1982.

845 Davis, G. L., Hart, S. R., and Tilton, G. R.: Some effects of contact metamorphism on zircon ages,
846 Earth and Planetary Science Letters, 5, 27–34, https://doi.org/10.1016/S0012-821X(68)80006-8,
847 1968.

848 Garber, J. M., Smye, A. J., Feineman, M. D., Kylander-Clark, A. R. C., and Matthews, S.:
849 Decoupling of zircon U–Pb and trace-element systematics driven by U diffusion in eclogite-facies
850 zircon (Monviso meta-ophiolite, W. Alps), Contrib Mineral Petrol, 175, 55,
851 https://doi.org/10.1007/s00410-020-01692-2, 2020.

852 Gehrels, G.: Detrital Zircon U-Pb Geochronology Applied to Tectonics, Earth and Planetary
853 Sciences, 42, 127 149, https://doi.org/10.1146/annurev-earth-050212-124012, 2014.

854 Geisler, T., Ulonska, M., Schleicher, H., Pidgeon, R. T., and van Bronswijk, W.: Leaching and
855 differential recrystallization of metamict zircon under experimental hydrothermal conditions,
856 Contrib Mineral Petrol, 141, 53–65, https://doi.org/10.1007/s004100000202, 2001.

857 Geisler, T., Pidgeon, R. T., Bronswijk, W. van, and Kurtz, R.: Transport of uranium, thorium, and
858 lead in metamict zircon under low-temperature hydrothermal conditions, Chemical Geology,
859 191, 141–154, https://doi.org/10.1016/s0009-2541(02)00153-5, 2002.

860 Geisler, T., Schaltegger, U., and Tomaschek, F.: Re-equilibration of Zircon in Aqueous Fluids and
861 Melts, Elements, 3, 43 50, https://doi.org/10.2113/gselements.3.1.43, 2007.

862 Grauert, B., Seitz, M. G., and Soptrajanova, G.: Uranium and lead gain of detrital zircon studied
863 by isotopic analyses and fission-track mapping, Earth and Planetary Science Letters, 21, 389–
864 399, https://doi.org/10.1016/0012-821X(74)90178-2, 1974.

865 Härtel, B., Jonckheere, R., Wauschkuhn, B., and Ratschbacher, L.: The closure temperature(s) of
866 zircon Raman dating, Geochronology, 3, 259–272, https://doi.org/10.5194/gchron-3-259-2021,
867 2021.

868 Hiess, J., Condon, D. J., McLean, N., and Noble, S. R.: 238U/ 235U systematics in terrestrial
869 uranium-bearing minerals, Science, 335, 1610 1614, 2012.

870 Hoskin, P. W. O. and Black, L. P.: Metamorphic zircon formation by solid-state recrystallization of
871 protolith igneous zircon, Journal of Metamorphic Geology, 18, 423 439,
872 https://doi.org/10.1046/j.1525-1314.2000.00266.x, 2002.

873 Jaffey, A. H., Flynn, K. F., Glendenin, L. E., Bentley, W. C., and Essling, A. M.: Precision
874 Measurement of Half-Lives and Specific Activities of U235 and U238, Physical Review C, 4,
875 1889–1906, https://doi.org/10.1103/physrevc.4.1889, 1971.

876 Kirkland, C. L., Abello, F., Danišík, M., Gardiner, N. J., and Spencer, C.: Mapping temporal and
877 spatial patterns of zircon U-Pb disturbance: A Yilgarn Craton case study, Gondwana Research,
878 52, 39 47, https://doi.org/10.1016/j.gr.2017.08.004, 2017.

879 Kirkland, C. L., Johnson, T. E., Kinny, P. D., and Kapitany, T.: Modelling U-Pb discordance in the
880 Acasta Gneiss: Implications for fluid–rock interaction in Earth's oldest dated crust, Gondwana
881 Research, 77, 223–237, https://doi.org/10.1016/j.gr.2019.07.017, 2020.

882 Kowallis, B. J., Ferguson, J., and Jorgensen, G. J.: Uplift along the salt lake segment of the
883 Wasatch fault from apatite and zircon fission track dating in the little Cottonwood stock,
884 International Journal of Radiation Applications and Instrumentation. Part D. Nuclear Tracks and
885 Radiation Measurements, 17, 325–329, https://doi.org/10.1016/1359-0189(90)90054-2, 1990.

886 Kusiak, M. A., Dunkley, D. J., Wirth, R., Whitehouse, M. J., Wilde, S. A., and Marquardt, K.:
887 Metallic lead nanospheres discovered in ancient zircons, Proceedings of the National Academy
888 of Sciences, 112, 201415264, https://doi.org/10.1073/pnas.1415264112, 2015.

889 Kusiak, M. A., Wirth, R., Wilde, S. A., and Pidgeon, R. T.: Metallic lead (Pb) nanospheres
890 discovered in Hadean and Eoarchean zircon crystals at Jack Hills, Sci Rep, 13, 895,
891 https://doi.org/10.1038/s41598-023-27843-6, 2023.

892 Lipp, A. and Vermeesch, P.: Short communication: The Wasserstein distance as a dissimilarity
893 metric for comparing detrital age spectra and other geological distributions, Geochronology, 5,
894 263–270, https://doi.org/10.5194/gchron-5-263-2023, 2023.

895 Massey, F. J.: The Kolmogorov-Smirnov Test for Goodness of Fit, Journal of the American
896 Statistical Association, 46, 68–78, https://doi.org/10.2307/2280095, 1951.

897 Matthews, W., Guest, B., and Madronich, L.: Latest Neoproterozoic to Cambrian detrital zircon
898 facies of western Laurentia, Geosphere, 14, 243–264, https://doi.org/10.1130/GES01544.1,
899 2017.

900 Mattinson, J., M.: Analysis of the relative decay constants of 235U and 238U by multi-step CA-
901 TIMS measurements of closed-system natural zircon samples, Chemical Geology, 275, 186–198,
902 https://doi.org/10.1016/j.chemgeo.2010.05.007, 2010.

903 McNaughton, N. J., Rasmussen, B., and Fletcher, I. R.: SHRIMP Uranium-Lead Dating of
904 Diagenetic Xenotime in Siliciclastic Sedimentary Rocks, Science, 285, 78–80,
905 https://doi.org/10.1126/science.285.5424.78, 1999.

906 Mezger, K. and Krogstad, E. J.: Interpretation of discordant U-Pb zircon ages: An evaluation,
907 Journal of Metamorphic Geology, 15, 127 140, https://doi.org/10.1111/j.1525-
908 1314.1997.00008.x, 1997.

909 Moore, J. N. and Kerrick, D. M.: Equilibria in siliceous dolomites of the Alta aureole, Utah,
910 American Journal of Science, 276, 502–524, https://doi.org/10.2475/ajs.276.4.502, 1976.

911   Morris, G. A., Kirkland, C. L., and Pease, V.: Orogenic paleofluid flow recorded by discordant
912   detrital zircons in the Caledonian foreland basin of northern Greenland, Lithosphere, 7, 138
913   143, https://doi.org/10.1130/l420.1, 2015.

914   Moser, D. E., Davis, W. J., Reddy, S. M., Flemming, R. L., and Hart, R. J.: Zircon U–Pb strain
915   chronometry reveals deep impact-triggered flow, Earth and Planetary Science Letters, 277, 73–
916   79, https://doi.org/10.1016/j.epsl.2008.09.036, 2009.

917   Moser, D. E., Cupelli, C. L., Barker, I. R., Flowers, R. M., Bowman, J. R., Wooden, J., and Hart, J. R.:
918   New zircon shock phenomena and their use for dating and reconstruction of large impact
919   structures revealed by electron nanobeam (EBSD, CL, EDS) and isotopic U–Pb and (U–Th)/He
920   analysis of the Vredefort domeThis article is one of a series of papers published in this Special
921   Issue on the theme of Geochronology in honour of Tom Krogh., Canadian Journal of Earth
922   Sciences, 48, 117 139, https://doi.org/10.1139/e11-011, 2011.

923   Nasdala, L., Pidgeon, R. T., Wolf, D., and Irmer, G.: Metamictization and U-PB isotopic
924   discordance in single zircons: a combined Raman microprobe and SHRIMP ion probe study,
925   Mineralogy and Petrology, 62, 1–27, https://doi.org/10.1007/BF01173760, 1998.

926   Nasdala, L., Hanchar, J. M., Rhede, D., Kennedy, A. K., and Váczi, T.: Retention of uranium in
927   complexly altered zircon: An example from Bancroft, Ontario, Chemical Geology, 269, 290 300,
928   https://doi.org/10.1016/j.chemgeo.2009.10.004, 2010.

929   Olierook, H. K. H., Kirkland, C. L., Barham, M., Daggitt, M. L., Hollis, J., and Hartnady, M.:
930   Extracting meaningful U-Pb ages from core–rim mixtures, Gondwana Research, 92, 102–112,
931   https://doi.org/10.1016/j.gr.2020.12.021, 2021.

932   Pidgeon, R. T., O'Neil, J. R., and Silver, L. T.: Uranium and Lead Isotopic Stability in a Metamict
933   Zircon under Experimental Hydrothermal Conditions, Science, 154, 1538–1540,
934   https://doi.org/10.1126/science.154.3756.1538, 1966.

935   Pidgeon, R. T., Nemchin, A. A., and Whitehouse, M. J.: The effect of weathering on U-Th-Pb and
936   oxygen isotope systems of ancient zircons from the Jack Hills, Western Australia, Geochimica et
937   Cosmochimica Acta, 197, 1 62, https://doi.org/10.1016/j.gca.2016.10.005, 2016.

938   Powerman, V. I., Buyantuev, M. D., and Ivanov, A. V.: A review of detrital zircon data treatment,
939   and launch of a new tool 'Dezirteer' along with the suggested universal workflow, Chemical
940   Geology, 583, 120437, https://doi.org/10.1016/j.chemgeo.2021.120437, 2021.

941   Rasmussen, K. L., Falck, H., Elongo, V., Reimink, J., Luo, Y., Pearson, D. G., Ootes, L., Creaser, R. A.,
942   and Lecumberri-Sanchez, P.: The source of tungsten-associated magmas in the northern
943   Canadian Cordillera and implications for the basement, Geology, 51, 657–662,
944   https://doi.org/10.1130/G51042.1, 2023.

945 Reddy, S. M., Timms, N. E., Trimby, P., Kinny, P. D., Buchan, C., and Blake, K.: Crystal-plastic
946 deformation of zircon: A defect in the assumption of chemical robustness, Geology, 34, 257 4,
947 https://doi.org/10.1130/g22110.1, 2006.

948 Reimink, J. R., Davies, J. H. F. L., Waldron, J. W. F., and Rojas, X.: Dealing with discordance: a
949 novel approach for analysing U–Pb detrital zircon datasets, Journal of the Geological Society,
950 173, 2015–114 585, https://doi.org/10.1144/jgs2015-114, 2016.

951 Resentini, A., Andò, S., Garzanti, E., Malusà, M. G., Pastore, G., Vermeesch, P., Chanvry, E., and
952 Dall'Asta, M.: Zircon as a provenance tracer: Coupling Raman spectroscopy and UPb
953 geochronology in source-to-sink studies, Chemical Geology, 555, 119828,
954 https://doi.org/10.1016/j.chemgeo.2020.119828, 2020.

955 Salje, E. K. H., Chrosch, J., and Ewing, R. C.: Is "metamictization" of zircon a phase transition?,
956 American Mineralogist, 84, 1107–1116, https://doi.org/10.2138/am-1999-7-813, 1999.

957 Schoene, B.: U–Th–Pb Geochronology, Elsevier, 2014.

958 Schoonover, E., Garber, J. M., Smye, A. J., Kylander-Clark, A., and Reimink, J. R.: Snapshots of
959 magmatic evolution revealed by zircon depth profiling, Earth and Planetary Science Letters, 647,
960 2024.

961 Seydoux-Guillaume, A.-M., Bingen, B., Paquette, J.-L., and Bosse, V.: Nanoscale evidence for
962 uranium mobility in zircon and the discordance of U–Pb chronometers, Earth and Planetary
963 Science Letters, 409, 43–48, https://doi.org/10.1016/j.epsl.2014.10.044, 2015.

964 Sharman, G. R. and Malkowski, M. A.: Modeling apparent Pb loss in zircon U–Pb geochronology,
965 Geochronology, 6, 37–51, https://doi.org/10.5194/gchron-6-37-2024, 2024.

966 Stacey, J. S. and Kramers, J. D.: Approximation of terrestrial lead isotope evolution by a two-
967 stage model, Earth and planetary science letters, 26, 207 221, https://doi.org/10.1016/0012-
968 821x(75)90088-6, 1975.

969 Stearns, M. A., Bartley, J. M., Bowman, J. R., Forster, C. W., Beno, C. J., Riddle, D. D., Callis, S. J.,
970 and Udy, N. D.: Simultaneous Magmatic and Hydrothermal Regimes in Alta–Little Cottonwood
971 Stocks, Utah, USA, Recorded Using Multiphase U-Pb Petrochronology, Geosciences, 10, 129,
972 https://doi.org/10.3390/geosciences10040129, 2020.

973 Trachenko, K., Dove, M. T., and Salje, E. K. H.: Large swelling and percolation in irradiated zircon,
974 J. Phys.: Condens. Matter, 15, L1, https://doi.org/10.1088/0953-8984/15/2/101, 2002.

975 Ulusoy, İ., Sarıkaya, M. A., Schmitt, A. K., Şen, E., Danišík, M., and Gümüş, E.: Volcanic eruption
976 eye-witnessed and recorded by prehistoric humans, Quaternary Science Reviews, 212, 187–198,
977 https://doi.org/10.1016/j.quascirev.2019.03.030, 2019.

978 Vermeesch, P.: On the visualisation of detrital age distributions, Chemical Geology, 312–313,
979 190 194, https://doi.org/10.1016/j.chemgeo.2012.04.021, 2012.

980 Vermeesch, P.: Dissimilarity measures in detrital geochronology, Earth-Science Reviews, 178,
981 310–321, https://doi.org/10.1016/j.earscirev.2017.11.027, 2018a.

982 Vermeesch, P.: IsoplotR: A free and open toolbox for geochronology, Geoscience Frontiers, 9,
983 1479 1493, https://doi.org/10.1016/j.gsf.2018.04.001, 2018b.

984 Vermeesch, P.: On the treatment of discordant detrital zircon U–Pb data, Geochronology, 3,
985 247–257, https://doi.org/10.5194/gchron-3-247-2021, 2021.

986 York, D.: Least squares fitting of a straight line with correlated errors, Earth and planetary
987 science letters, 5, 320 324, https://doi.org/10.1016/s0012-821x(68)80059-7, 1968.

988 Zhang, M., Salje, E. K. H., Farnan, I., Graeme-Barber, A., Daniel, P., Ewing, R. C., Clark, A. M., and
989 Leroux, H.: Metamictization of zircon: Raman spectroscopic study, J. Phys.: Condens. Matter, 12,
990 1915, https://doi.org/10.1088/0953-8984/12/8/333, 2000.

991 Zi, J.-W., Rasmussen, B., Muhling, J. R., and Fletcher, I. R.: In situ U-Pb and geochemical evidence
992 for ancient Pb-loss during hydrothermal alteration producing apparent young concordant zircon
993 dates in older tuffs, Geochimica et Cosmochimica Acta, 320, 324–338,
994 https://doi.org/10.1016/j.gca.2021.11.038, 2022.

995